NUMERICAL ANALYSIS OF EMBANKMENT FOUNDATION LIQUEFACTION COUNTERMEASURES

AHMED ELGAMAL

Department of Structural Engineering, University of California,
San Diego, 9500 Gilman Dr., La Jolla, CA 92093, USA

ENDER PARRA

PDVSA, INTEVEP, Urbanización Santa Rosa, Los Teques,
P.O. Box 76343A, Caracas 1070A, Venezuela

ZHAOHUI YANG

Department of Structural Engineering, University of California,
San Diego, 9500 Gilman Dr., La Jolla, CA 92093, USA

KORHAN ADALIER

Department of Civil Engineering, Rensselaer Polytechnic Institute,
Troy, NY 12180, New York, USA

Computational simulations are presented for a unique series of centrifuge tests conducted to assess the performance of liquefaction countermeasure techniques. In these centrifuge tests, the dynamic response of an embankment supported on a liquefiable foundation (medium sand) is investigated. The experimental series included: (i) a benchmark test without a liquefaction countermeasure, (ii) foundation densification below the embankment toe, and (iii) use of a sheet-pile containment enclosure below the embankment. This series of experiments documents a wide range of practical liquefaction response mechanisms (including countermeasure implementation). In order to numerically simulate the above centrifuge tests, a new calibrated soil stress-strain constitutive model is incorporated into a two-phase (solid-fluid) fully coupled Finite Element formulation. Comparison of the computational and experimental results demonstrates: (i) importance of post-liquefaction dilative soil behavior in dictating the dynamic response and deformation characteristics of the embankment-foundation system, and (ii) capabilities and limitations of the numerical modeling procedure.

Keywords: Liquefaction; countermeasures; lateral spreading; embankment; centrifuge; dilation; plasticity; coupled formulation.

1. Introduction

Soil structures such as river dikes, highway embankments, and earth dams have been frequently damaged during past major earthquakes. This damage was often mainly due to liquefaction of the embankment and/or foundation soils [Seed, 1968; 1970;

Matsuo, 1996]. In most cases, large deformations occurred due to liquefaction of the supporting loose cohesionless foundation soil [Seed, 1968; Tani, 1996], resulting in cracking, settlement, lateral spreading, and slumping. Liquefaction of embankment and river dike foundations was reported during the 1960 Alaskan earthquake [McCulloch and Bonilla, 1967; Seed, 1970], the 1964 Niigata, Japan earthquake [Kawakami and Asada, 1966], the 1983 Nipponkai-Chubu, Japan earthquake [Tani, 1991], among many others. As a result of the 1995 Hyogoken-Nanbu (Kobe) earthquake, nearly 1200 small earth embankments (80less) suffered some level of damage [Tani, 1996; Matsuo, 1996].

Such earthquake liquefaction hazard necessitates the development of appropriate remediation countermeasures [Ledbetter *et al.*, 1994; Marcuson *et al.*, 1996]. In order to experimentally investigate this problem, researchers frequently resort to the centrifuge geotechnical modelling technique. This technique involves subjecting a small-scale model to a high level of confinement by the action of a centrifuge-induced gravitational field (e.g., 75 times the confinement due to earth gravity (g), at $75g$). In this fashion, the small model mechanically represents a much larger prototype (e.g., 75 times larger in linear dimensions at $75g$), due to dependence of soil response on confinement. Centrifuge modeling data sets play a major role in verification and refinement of liquefaction countermeasures [Arulanandan and Scott, 1993; 1994; Kimura *et al.*, 1997]. Such data also provides a basis for calibration of design and computational modeling procedures [Finn *et al.*, 1994; Marcuson *et al.*, 1996].

As such, the effort reported in this paper is focused on computational modeling of a series of centrifuge tests [Adalier, 1996; Adalier *et al.*, 1998]. In this test series, performance of countermeasure techniques for a liquefiable embankment foundation was assessed experimentally. Using this valuable test data, the conducted numerical study attempted to investigate and shed light on the underlying dynamic response mechanisms. The employed soil stress-strain (constitutive) model was calibrated earlier [Parra, 1996] for the liquefiable embankment foundation soil (Nevada Sand at a relative density D_r of about 40%). In order to conduct numerical simulations, the constitutive model was incorporated into a solid-fluid fully coupled Finite Element (FE) code. Using this code, the computed response was compared to the corresponding experimental results. Herein, emphasis is placed on demonstrating: (i) salient pre- and post-liquefaction foundation response characteristics (original and remediated), observed both computationally and experimentally, and (ii) capabilities and limitations of the employed computational framework.

This study may be viewed as a component of earlier and ongoing efforts to develop appropriate numerical models for simulation/prediction of liquefaction-induced ground response [e.g., Finn *et al.*, 1977; Nemat-Nasser and Shokooh, 1979; Prevost, 1985; 1989; Wang *et al.*, 1990; Iai, 1991; Arulanandan and Scott, 1993; 1994; Muraleetharan *et al.*, 1994; Byrne and McIntyre, 1994; Manzari and Dafalias, 1997; Cubrinovski and Ishihara, 1998; Borja *et al.*, 1999a; 1999b; Li and Dafalias, 2000; Pecker *et al.*, 2001]. In the following, we start with a summary of the experi-

mental program, and the employed numerical framework (the FE formulation and soil constitutive model). Results of the numerical simulations are then presented and compared to the experimental response. All computational and experimental data are reported in prototype scale [Tan and Scott, 1985].
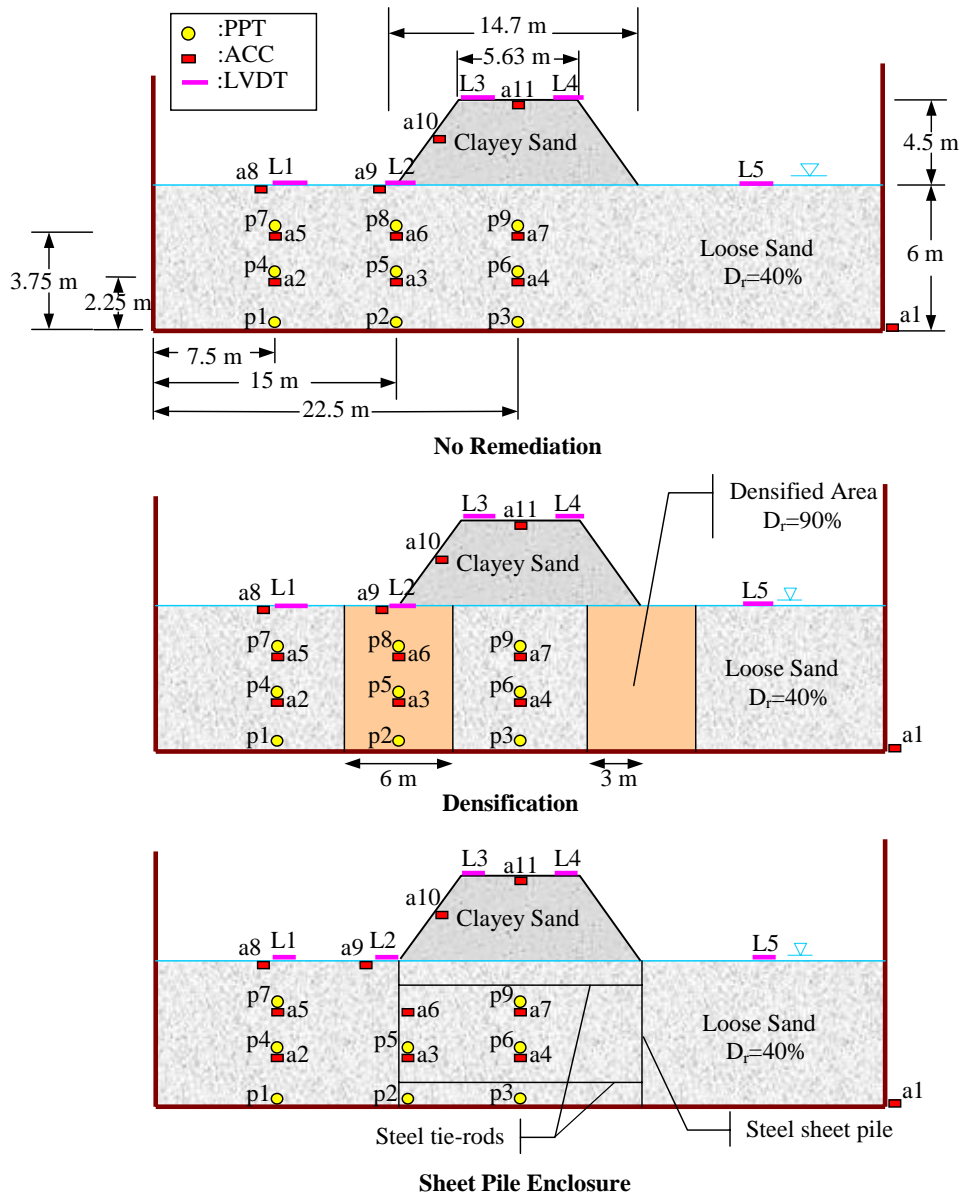

Fig. 1. Centrifuge model setup ([Adalier *et al.*, 1998], PPT is Pore-Pressure Transducer, ACC is Accelerometer, LVDT is Linear Variable Differential Transducer to measure displacement).

2. Centrifuge Testing Program

The liquefaction countermeasure experimental study was conducted [Adalier, 1996; Adalier *et al.*, 1998] at Rensselaer Polytechnic Institute. Dynamic stability of a 4.5 m clayey sand embankment supported on 6 m of medium saturated sand (Fig. 1) was systematically tested in a $75g$ centrifugal acceleration field (the models were 20 m in thickness). The embankment was built at 1:1 slopes, composed of a Kaolin clay and Nevada 120 sand mixture (1:4 weight ratio) with a mass density of 1900 kg/m³ and a water content of 14%. Nevada 120 fine sand [Arulmoli *et al.*, 1992] was used as the liquefiable foundation soil (at $D_r \approx 40\%$). The foundation layer was saturated with a pore fluid at a prototype permeability coefficient of 5.5×10^{-4} m/s, within the range of medium sands [Lambe and Whitman, 1969].
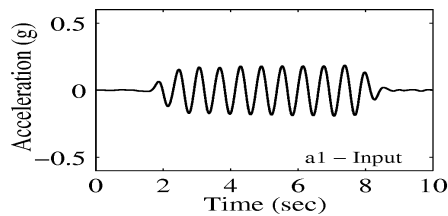

Fig. 2.   Recorded input motion (typical form).

As seen in Fig. 1, the first model constituted the benchmark case with no remedial work [Adalier, 1996]. In the second model, 6 m wide densified areas were placed under the embankment toes (reaching $D_r \approx 90\%$, according to *in-situ* applications). Finally, in the third model, two steel sheet piles were tied together (with four steel tie-rods), and placed in the foundation layer below the embankment [see Kimura *et al.*, 1997 for a similar application]. The sheet piles were perforated in order to facilitate drainage in the horizontal direction. One dimensional (1D) horizontal shaking was imparted along the model long axis. Each model was shaken at about $0.18g$ peak excitation, with a uniform harmonic base input motion of 10 cycles at 1.6 Hz (Fig. 2). The response was monitored (Fig. 1) by accelerometers (ACC), pore pressure transducers (PPT), and Linear Variable Differential Transformers (LVDT) to measure displacement.

3. Numerical Modelling Procedure

In order to study the dynamic response of saturated soil systems as an initial-boundary-value problem, a two-dimensional plane-strain FE program was developed [Parra, 1996; Yang, 2000]. This program implements the two-phase (solid-fluid) fully coupled FE formulation of Chan [1988] and Zienkiewicz *et al.* [1990], and incorporates a soil liquefaction constitutive model [Parra, 1996; Yang, 2000]. In the following sections, the employed FE formulation and stress-strain model are summarised.

3.1. *Finite element formulation*

The saturated soil system is modeled as a two-phase material based on the Biot [1962] theory for porous media. A simplified numerical formulation of this theory, known as *u-p* formulation (in which displacement of the soil skeleton *u*, and pore pressure *p*, are the primary unknowns, [Chan, 1988; Zienkiewicz *et al.*, 1990]), was implemented numerically [Ragheb, 1994; Parra, 1996; Yang, 2000]. The *u-p* formulation is defined by [Chan, 1988]: (i) equation of motion for the solid-fluid mixture, and (ii) equation of mass conservation for the mixture, incorporating equation of motion for the fluid phase and Darcy's law. In the finite element context, these governing equations may be expressed in the following matrix form [Chan, 1988]:

$$\mathbf{M\ddot{U}} + \int_{\mathbf{\Omega}} \mathbf{B^T}\boldsymbol{\sigma'}\mathbf{d\Omega} + \mathbf{Qp} - \mathbf{f^s} = \mathbf{0} \tag{1a}$$

$$\mathbf{Q^T\dot{U}} + \mathbf{S\dot{p}} + \mathbf{Hp} - \mathbf{f^p} = \mathbf{0} \tag{1b}$$

where $\mathbf{M}$ is the mass matrix, $\mathbf{U}$ the displacement vector, $\mathbf{B}$ the strain-displacement matrix, $\boldsymbol{\sigma'}$ the effective stress vector (determined by the soil constitutive model discussed below), $\mathbf{Q}$ the discrete gradient operator coupling the solid and fluid phases, $\mathbf{p}$ the pore pressure vector, $\mathbf{H}$ the permeability matrix, and $\mathbf{S}$ the compressibility matrix. The vectors $\mathbf{f^s}$ and $\mathbf{f^p}$ include the effects of body forces and the prescribed boundary conditions for the solid and fluid phases respectively. In Eq. (1a), the first term represents inertia force of the solid-fluid mixture, followed by internal force due to soil skeleton deformation, and internal force induced by pore-fluid pressure. In Eq. (1b), the first two terms are the rates of volume change with time for the soil skeleton and the fluid phase respectively, followed by seepage rate of the pore fluid ($\mathbf{Hp}$).

Equations (1) are integrated in time using a single-step predictor multi-corrector scheme of the Newmark type [Chan, 1988; Parra, 1996]. The solution is obtained for each time step using the modified Newton-Raphson approach [Parra, 1996].

A typical element employed in the *u-p* formulation is shown in Fig. 3, with nine nodes for the solid phase and four nodes for the fluid phase, so as to reduce numerical difficulties associated with the nearly incompressible fluid phase [Chan, 1988]. Each solid node is associated with two-degrees-of-freedom (2 DOF) for the lateral and vertical displacements, and each fluid node is associated with 1 DOF for pore pressure. This 9-4-node element is employed in all numerical simulations presented herein.

3.2. *Constitutive model*

In the employed soil constitutive model, emphasis is placed on controlling the magnitude of liquefaction-induced cycle-by-cycle shear strain accumulation in clean
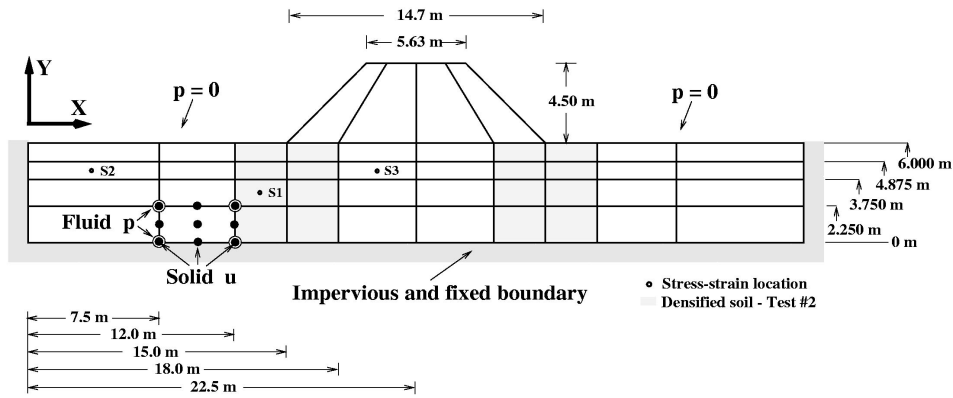
Fig. 3.   Finite element discretisation and boundary conditions (modified from Parra [1996]).
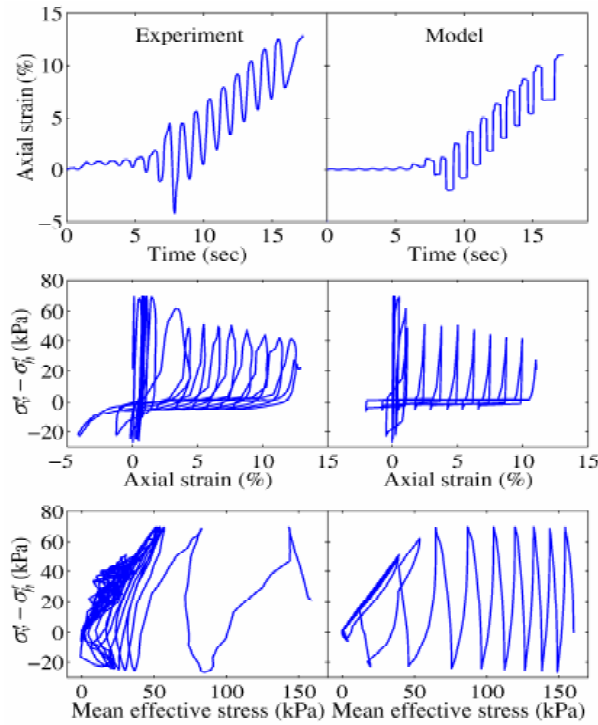

Fig. 4.   Recorded and computed results of anisotropically consolidated, undrained cyclic triaxial test (Nevada sand at 40% relative density) with static stress bias [Arulmoli *et al.*, 1992; Yang, 2000].

medium-dense sands [Parra, 1996; Yang, 2000; Elgamal *et al.*, 2001]. The experimentally observed accumulation of permanent deviatoric strain (e.g., Fig. 4, [Arulmoli *et al.*, 1992]) was modelled as a distinct phase, within the framework of multi-surface plasticity [Prevost, 1985]. Furthermore, appropriate loading-unloading flow

rules were devised to reproduce the strong dilation tendency seen in Fig. 4, which results in increased shear stiffness and strength (at large cyclic shear strain excursions). The main components of this model are summarised below [Parra, 1996; Yang, 2000; Elgamal *et al.*, 2001].

3.2.1. *Yield function*

Following the classical plasticity convention [Hill, 1950], it is assumed that material elasticity is linear and isotropic, and that nonlinearity and anisotropy result from plasticity. The selected yield function [Prevost, 1985; Lacy, 1986] forms a conical surface in stress space with its apex at $(-p'_0)$ along the hydrostatic axis (Fig. 5). In the context of multi-surface plasticity [Iwan, 1967; Mroz, 1967; Prevost, 1985], a number of similar yield surfaces with a common apex and different sizes form the hardening zone (Fig. 5). The outermost surface is the envelope of peak shear strength (failure envelope).
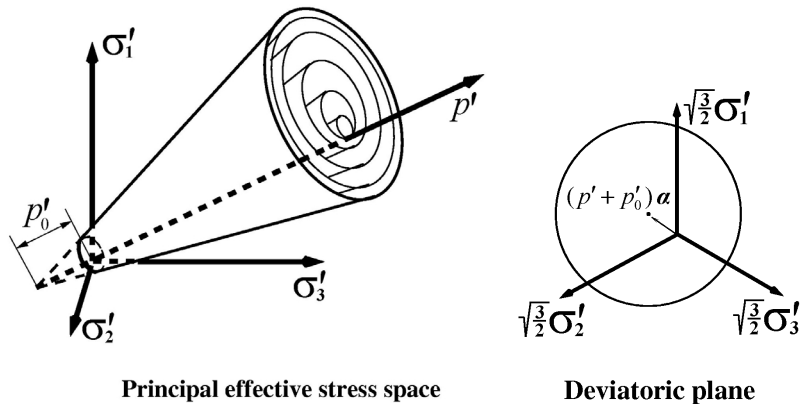

Principal effective stress space **Deviatoric plane**

Fig. 5. Conical yield surface in principal stress space and deviatoric plane (after Prevost [1985], Parra [1996] and Yang [2000]).

3.2.2. *Hardening rule*

A purely deviatoric kinematic hardening rule [Prevost, 1985] is employed in order to generate hysteretic response under cyclic shear loading. This kinematic rule dictates that all yield surfaces may translate in stress space within the failure envelope [Hill, 1950].

3.2.3. *Flow rule*

During shear loading, the soil contractive/dilative behaviour is handled by a non-associative flow rule [Parra, 1996; Elgamal *et al.*, 2001] so as to achieve appropriate interaction between shear and volumetric response. In particular, nonassociativity
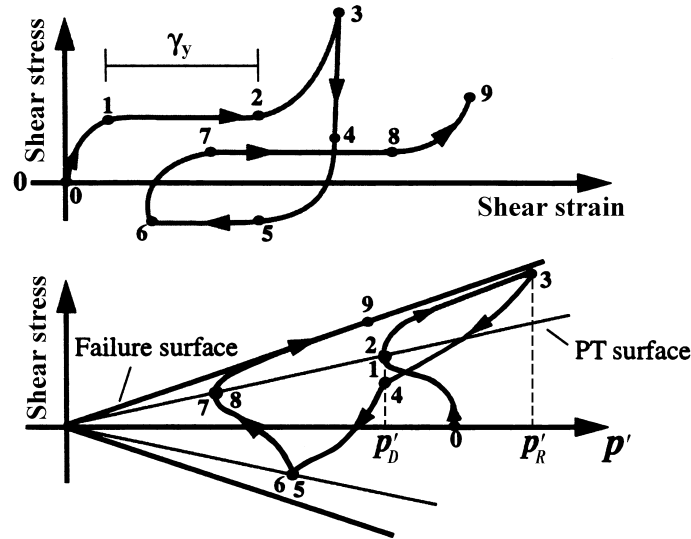
Fig. 6.   Schematic of undrained constitutive model response showing shear stress, effective confinement, and shear strain relationship.

is restricted to the volumetric component $\mathbf{P}''$ of the plastic flow tensor (outer normal to the plastic potential surface in stress-space). Therefore, depending on the relative location of the stress state (Fig. 6) with respect to the *phase transformation* (PT) surface [Ishihara, 1985; Vaid and Thomas, 1995; Vaid and Sivathayalan, 1999; Iai, 1991; Kramer, 1996; Dobry and Abdoun, 1998], different expressions for $\mathbf{P}''$ were specified for [Parra, 1996]:

(1) The contractive phase within the PT surface (Fig. 6, phase 0–1),
(2) The dilative phase during shear loading, with the stress state outside the PT surface (Fig. 6, phase 2–3). This phase ends when either fluid cavitation occurs [Casagrande, 1975; Iai, 1998] or the critical state is reached [Manzari and Dafalias, 1997; Li and Dafalias, 2000].
(3) The contractive phase during shear unloading (Fig. 6, phase 3–4), until the effective confinement returns to p'_D, and
(4) The liquefaction-induced perfectly plastic phase during shear loading (Fig. 6, phase 1–2), before the initiation of dilation (Fig. 6, phase 2-3). This phase is significant only at very low confinement (e.g., below 10 kPa for Nevada Sand), where considerable permanent shear strain (γ_y) may accumulate with minimal change in shear stress. Specification of this distinct yield phase allows direct control over its extent according to experimental observations (Fig. 4).

In summary, the main modelling parameters include typical dynamic soil properties such as low-strain shear modulus and friction angle, as well as calibration constants to control pore-pressure buildup rate, dilation tendency, and the level of liquefaction-induced cyclic shear strain.

3.2.4. *Model calibration*

The employed model has been extensively calibrated for the embankment foundation material — clean Nevada sand at $D_r \approx 40\%$ [Parra, 1996; Yang, 2000]. The calibration phase included results of monotonic and cyclic laboratory tests (Arulmoli *et al.* [1992], Fig. 4), as well as data from level-ground and mildly inclined infinite-slope dynamic centrifuge-model simulations [Taboada, 1995; Dobry *et al.*, 1997].

In the following numerical studies, this calibrated sand model was employed throughout to represent the dynamic properties of the foundation soil. For Nevada sand at about 40% relative density, the stiffness was represented by a low-strain shear modulus of 31.4 MPa at 80 kPa confinement, and the shear strength corresponded to a friction angle of 31 degrees. The phase transformation angle was 26 degrees, with a γ_y of 1.0%. For the embankment, material properties were defined as a cohesion of 25 kPa and a friction angle of 32° (a simplified version of the same constitutive model was used).

3.3. *Finite element model setup*

The finite-element mesh for the embankment-foundation system is shown in Fig. 3. Boundary conditions for all simulations were [Parra, 1996]:

(1) For the solid phase, horizontal input motion was specified along the base and the two lateral sides, as the recorded rigid container acceleration (Fig. 2). All base nodes were fixed in the vertical direction. Along the lateral sides, vertical motion was allowed.
(2) For the fluid phase, the base and the two sides (i.e., the container boundaries) were impervious (zero flow rate, which is a natural boundary condition). In addition, zero pore pressure was prescribed along the foundation surface (at the water-table level) and within the entire embankment.

4. Computation Results and Discussion

During the computational simulations, soil stress-strain responses were sampled at S1, S2 and S3 locations as shown in Fig. 3 [Parra, 1996]. These locations were selected to represent zones of different response characteristics, namely: (i) S1 below the embankment toe, (ii) S3 below the embankment (near centerline) where vertical confinement is highest, and (iii) S2 in the free field away from the supported embankment. At these key locations, computed accelerations, pore-pressures and vertical settlement will be compared to the corresponding measurements.

4.1. *Embankment on medium Nevada sand (benchmark test)*

The imparted cycles of dynamic excitation (Fig. 2) resulted in the deformed configuration of Fig. 7, with peak vertical and lateral displacements of about 0.25 m.
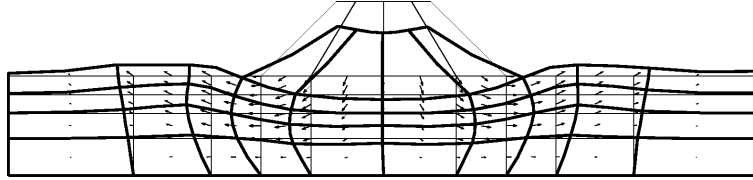
Fig. 7.   Computed deformed configuration (no remediation, deformations magnified by a factor of 6 for clarity).

Primarily, the deformation pattern shows: (i) major lateral displacement and shear below the embankment toe in the foundation soil (which liquefied due to the imparted dynamic excitation), and (ii) relatively mild lateral shear below the symmetric embankment center. These two deformation mechanisms are discussed below in terms of soil stress/strain response.

4.1.1. *Below embankment toe*

The deformation in Fig. 7 was associated with a large permanent lateral shear strain under the toe of 6% (Fig. 8, location S1), which clearly shows the mechanisms of: (i) cycle-by-cycle shear strain accumulation, and (ii) gradual loss of shear strength. The associated stress-path (Fig. 9) shows a major reduction in confinement during the first 3 cycles of shaking (due to excess-pore pressure buildup), followed by cycles of significant dilative response (stress-path along failure surface). The asymmetric
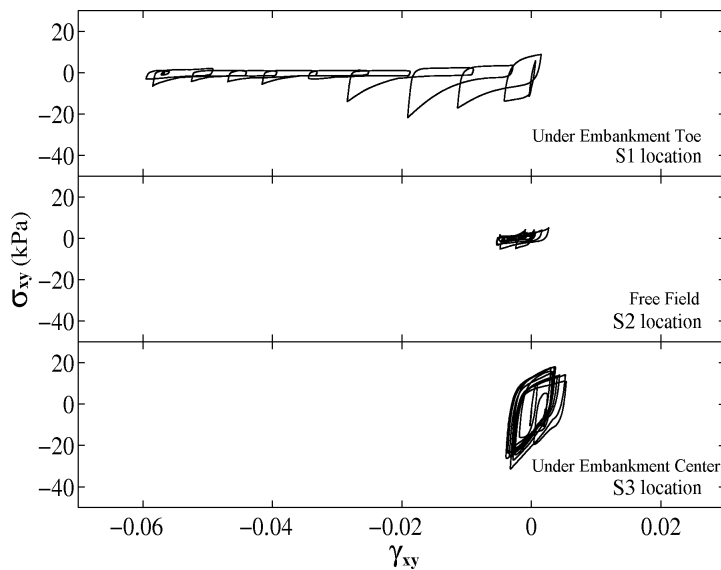

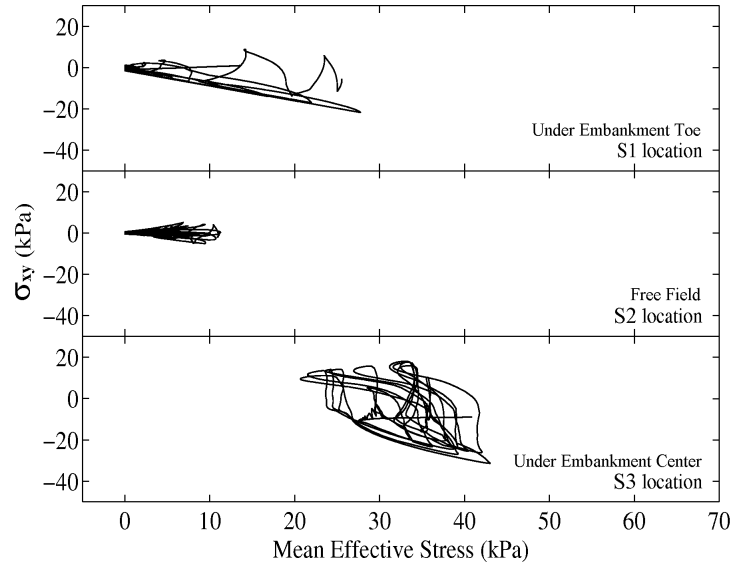Fig. 8.   Computed shear stress-strain histories (no remediation).

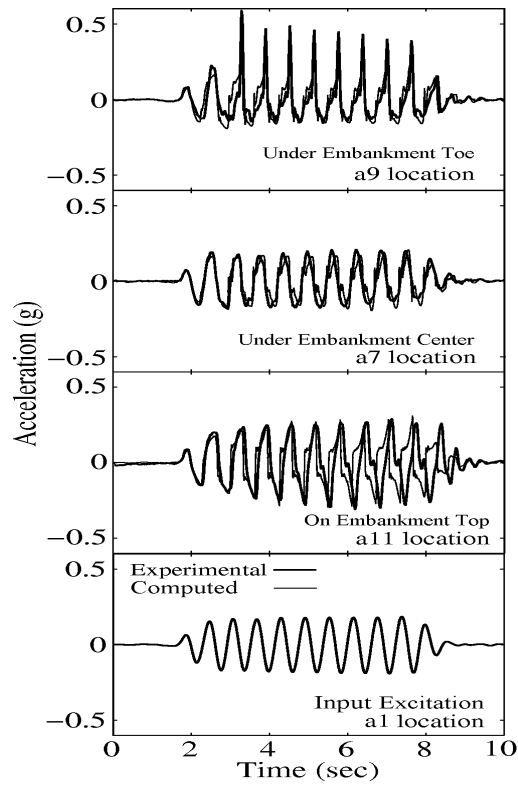Fig. 9.   Computed effective stress path (no remediation).

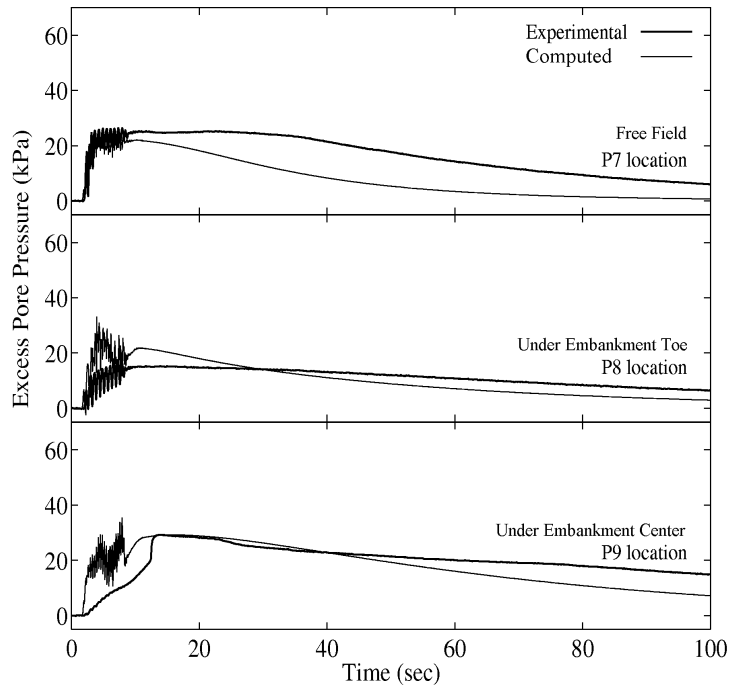Fig. 10.   Computed and experimental lateral acceleration histories (no remediation).

Fig. 11.   Computed and experimental excess pore-pressure histories (no remediation).

phases of dilative response (in the "down-slope" direction) instantaneously increase the soil shearing resistance, resulting in a pattern of strong asymmetric acceleration spikes, as exhibited both computationally and experimentally (Fig. 10, a9 location compared to a1 input). At this location, the computed and experimental pore-pressure histories were in reasonable agreement (Fig. 11, P8 location).

4.1.2. *Below embankment center*

The computed lateral shear stress-strain response at this location shows (S3 in Fig. 8): (i) minimal cycle-by-cycle permanent shear strain accumulation, and (ii) no substantial loss in shear stiffness throughout the shaking phase. Higher effective confinement due to embankment weight appears to have sustained pore-pressure well below the level of liquefaction (P9 in Fig. 11, both computed and experimental). The corresponding stress path indicates that (S3 in Fig. 9): (i) the dilation phase was apparent with minimal accumulated shear strain compared to S1 location under the embankment toe, and (ii) the maximum loss in effective confinement was only one half of the initial value of about 40 kPa. Absence of major "down-slope" response at this location dictated an essentially symmetric acceleration response (a7 in Fig. 10).

Finally, the computed shear stress and strain responses in the free field (S2 in Figs. 8 and 9) show the typical cyclic loss of shear stiffness and strength due to

liquefaction. At this location, initial confinement was low, and the free-field response was characterized by low-amplitude (symmetric) cycles of shear strain. These cycles led to rapid pore-pressure buildup and liquefaction (P7 in Fig. 11).

4.2. *Remediation by densification*

In this case, the sand columns below the embankment toe (shaded areas in Figs. 1 and 3) were densified to a high D_r of about 90% (actual field densification procedures will typically achieve this high D_r as an upper bound [Adalier, 1996]). As no experimental data was available for Nevada sand at this high relative density, model parameters were defined [Parra, 1996] based on the available data for Nevada sand at D_r of 40% and 60% [Arulmoli *et al.*, 1992], as well as other empirical dense sand properties [Lambe and Whitman, 1969]. Thus, the material properties at $D_r = 90\%$ were representative of a stiff and much less liquefiable sand (soil friction angle of 38°).

In the presence of the densified zones, the computed deformed configuration (Fig. 12) shows a pattern similar to the case of no remediation (Fig. 7), but with smaller lateral displacements and shear under the embankment toe (only 0.15 m compared to 0.25 m without remediation). The associated stress/strain response characteristics below the embankment toe and embankment center are summarised below.
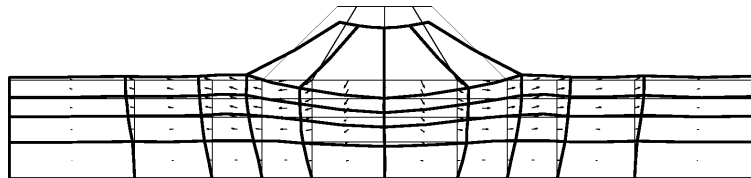

Fig. 12.   Computed deformed configuration (remediation by densification, deformations magnified by a factor of 6 for clarity).

4.2.1. *Below embankment toe*

The smaller lateral deformation at this location was associated with significant cyclic dilation tendency in the dense sand, as indicated by (S1 in Fig. 13): (i) phases of sharp increase in shear stiffness and strength, and (ii) lower cyclic shear strain accumulation in each shaking cycle. The corresponding stress path (S1 in Fig. 14) also shows instantaneous regains in shear strength and effective confinement that are significantly more pronounced (compare S1 in Figs. 9 and 14). These major dilative stress excursions within the densified material also resulted in: (i) strong asymmetric acceleration spikes manifested both experimentally and numerically (Fig. 15, a9 compared to a1), and (ii) computed dilation-induced phases of sharp pore-pressure drops (Fig. 16, P8). It is noted here that the magnitude of these
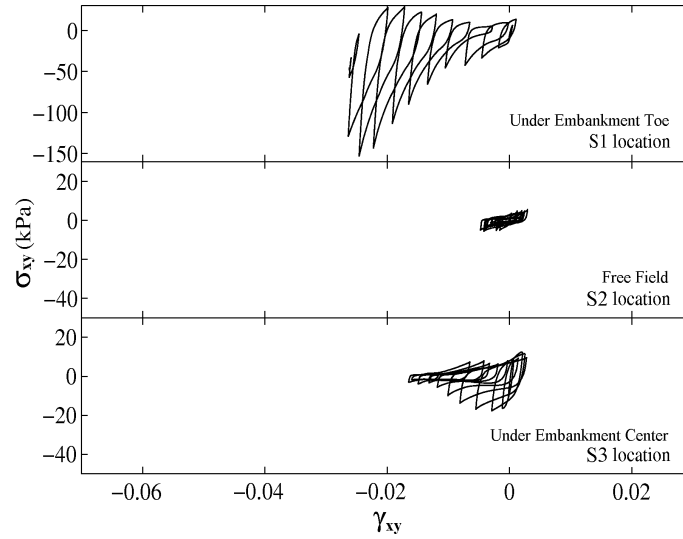
Fig. 13.   Computed shear stress-strain histories (remediation by densification).
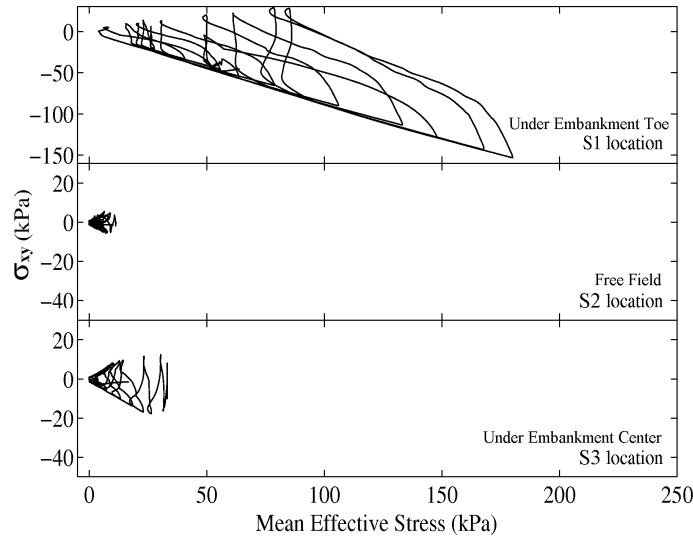

Fig. 14.   Computed effective stress path (remediation by densification).

drops cannot be compared to the experimental results, in which the employed pore-pressure transducers were physically unable to respond to such abrupt fluctuations (verified in independent tests of the transducer [Adalier, 1996]).

4.2.2. *Below embankment center*

The densified zones provided significant overall foundation strength, and contained the loose sand stratum below the embankment center. At this location, contractive
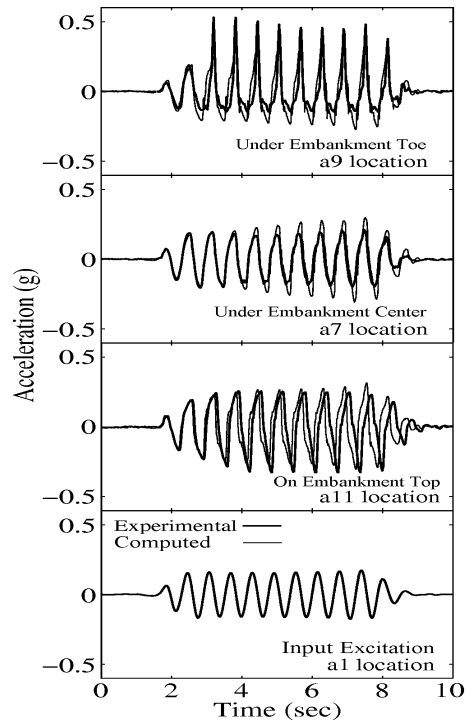
Fig. 15. Computed and experimental lateral acceleration histories (remediation by densification).
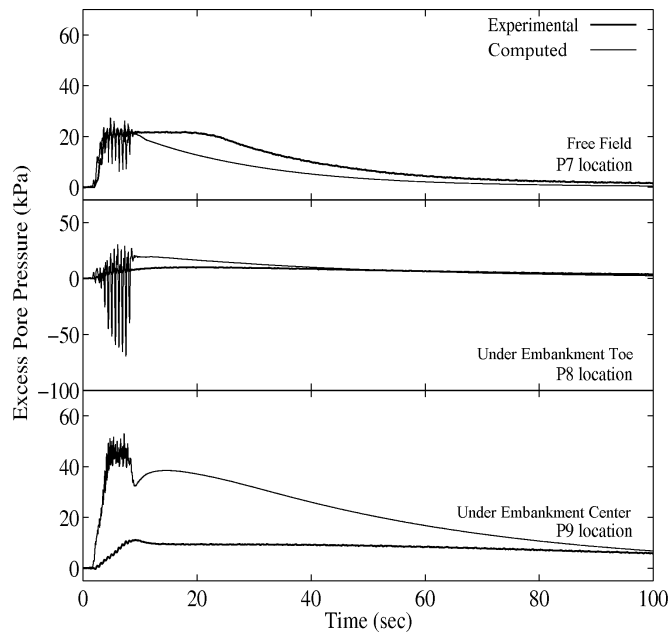

Fig. 16. Computed and experimental excess pore-pressure histories (remediation by densification).

response is seen to dominate (S3 in Figs. 13 and 14), resulting in the typical pattern of cyclic loss of shear stiffness (Fig. 13) and effective confinement (Fig. 14). The essentially symmetric computed and recorded acceleration histories are seen to be in reasonable agreement (a7 in Fig. 15). However, significant discrepancy was observed between computed and recorded pore-pressures (P9 in Fig. 16). This discrepancy points to computational limitations and will be discussed further in a later section. Finally, the free field is seen to display the typical loss of stiffness and strength due to liquefaction (S2 in Figs. 13 and 14). At this location the response is essentially identical to the earlier no-remediation case (S2 in Figs. 8 and 9).

4.3. *Remediation by sheet-pile enclosure*

Kimura *et al.* [1997] found containment sheet-piles with drainage capability to be a most effective countermeasure. A similar conclusion was also reached by Adalier [1996] based on experimental observations. Essentially, this retrofit procedure resulted in perfect containment of the foundation soil below the embankment (Fig. 1). Numerically, lateral deformations were also virtually nonexistent (Fig. 17). In this numerical simulation, the sheet-pile system was not directly modelled. Instead, the horizontal nodal degrees of freedom at the sheet-pile locations (Fig. 3) were tied together (using a penalty method). This constraint results in identical displacement at the sheet-pile locations, and prevents the enclosed foundation soil from flowing into the free field.
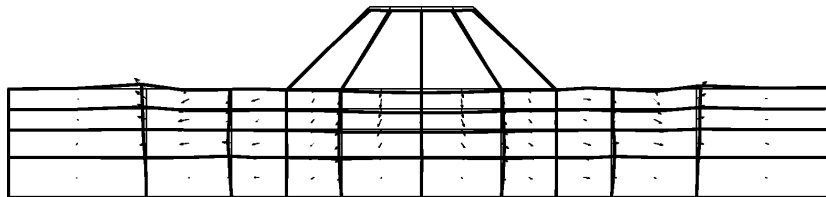

Fig. 17.   Computed deformed configuration (remediation by sheet-pile enclosure, deformations magnified by a factor of 6 for clarity).

As a result of this containment remediation, soil stress-strain response remained in the relatively small strain range, with predominantly contractive behaviour at all sampled locations (Figs. 18 and 19). The reduction in shear stiffness and strength (Fig. 18) is manifested in the computed and recorded accelerations, which show a decay in amplitude everywhere (Fig. 20). It may be argued in this case, that computational modelling of dilative response was only of marginal significance, compared to its major (or even critical) importance in the first two model simulations. Finally, significant discrepancy (P9 in Fig. 21) may be noted in the recorded and computed pore-pressure below the embankment (see further discussion in later sections).
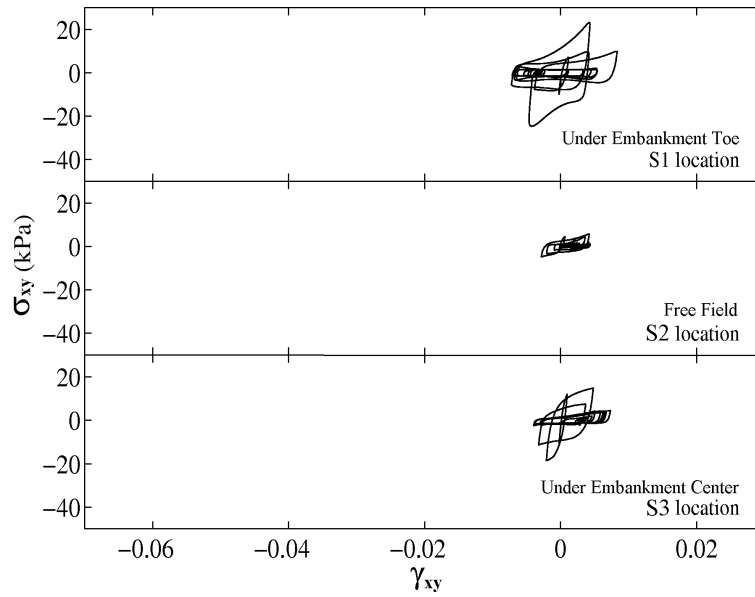
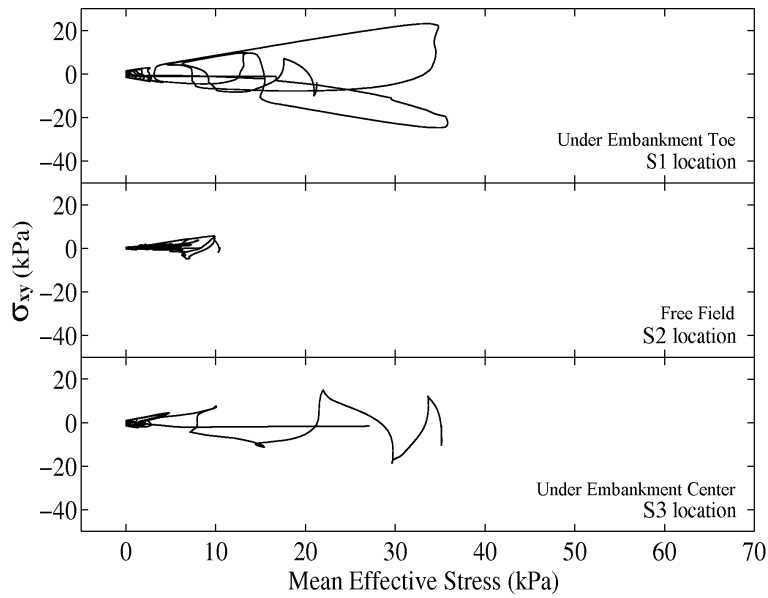Fig. 18. Computed shear stress-strain histories (remediation by sheet-pile enclosure).

Fig. 19. Computed effective stress path (remediation by sheet-pile enclosure).
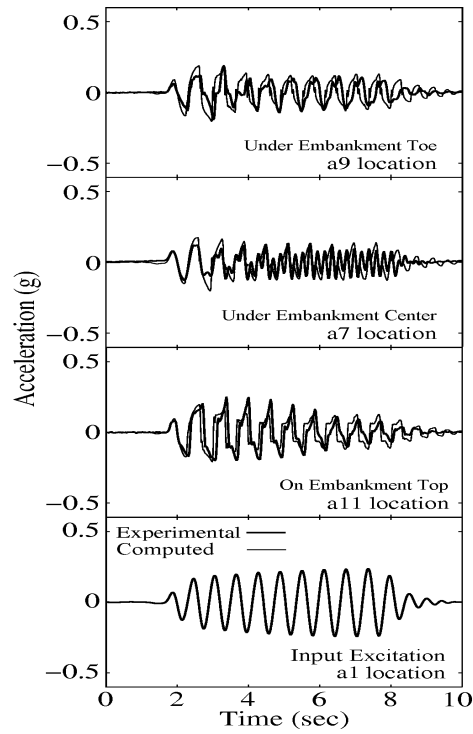
Fig. 20.   Computed and experimental lateral acceleration histories (remediation by sheet-pile enclosure).
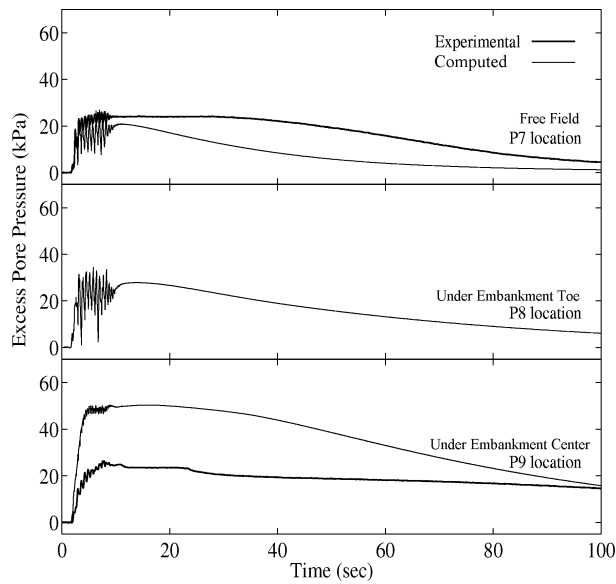

Fig. 21.   Computed and experimental excess pore-pressure histories (remediation by sheet-pile enclosure).

4.4. *Comparison of vertical settlements*

4.4.1. *No remediation*

Both ground surface and embankment settled at a nearly uniform rate (Fig. 22) during the shaking phase. The embankment was observed to undergo large settlements of approximately 2.5 cm per cycle of base excitation (Fig. 22, L3). These settlements were partially a result of migration of underlying foundation soil towards the free field (lateral spreading), as indicated by a computed heave of as much as 11 cm at the free field surface (Fig. 22, L1). However, the experimental results at L1 showed a net settlement of 4 cm, reflecting possibly the effect of soil densification due to the shaking process (which was not adequately accounted for by the numerical model). In general, additional deformations after the shaking phase were negligible.

4.4.2. *Remediation by densification*

Since the densified zones were able to limit lateral migration of foundation soil towards the free field, both computed and observed embankment surface settlements were reduced significantly (Fig. 23, L3). Computed vertical displacement at the free field surface (Fig. 23, L1) showed a net heave of 4 cm, compared to 11 cm above
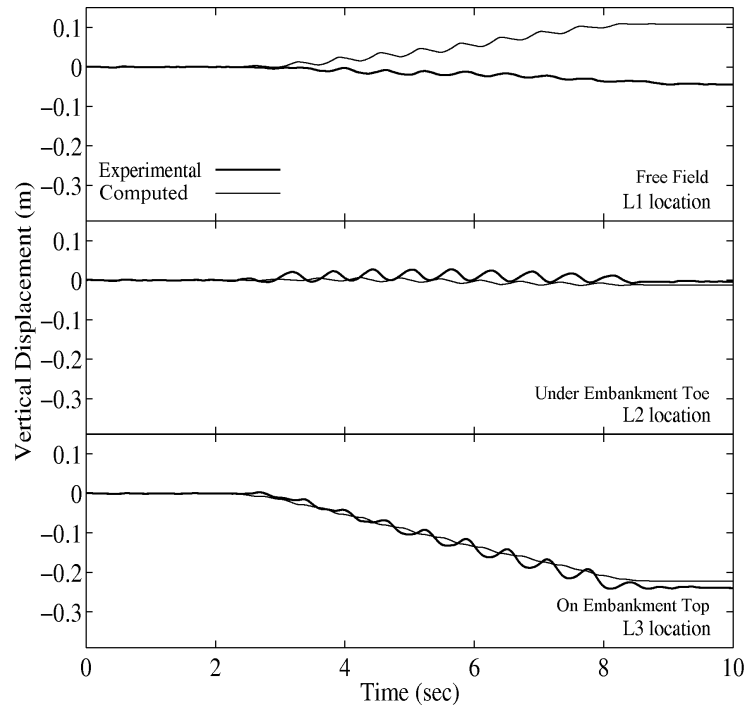

Fig. 22.   Computed and experimental vertical settlement time histories (no remediation).
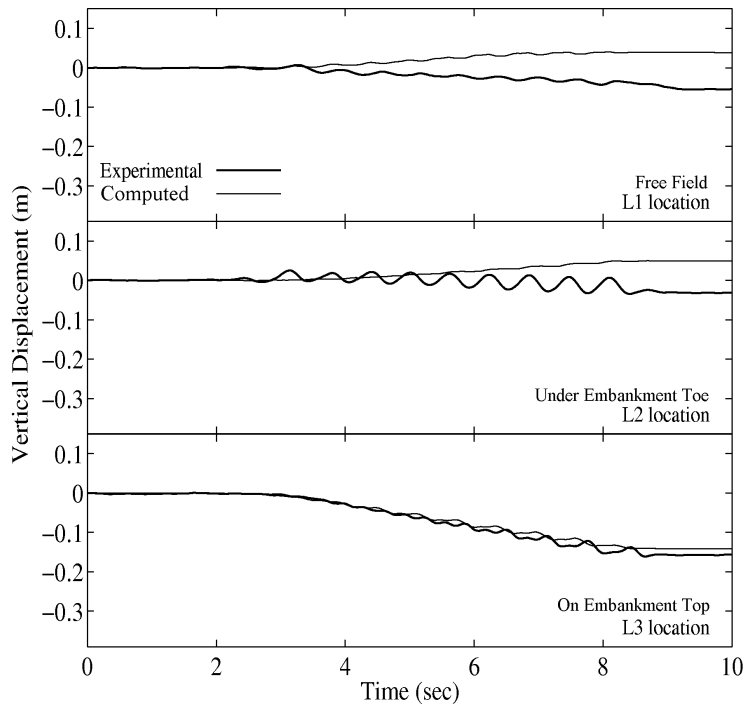
Fig. 23. Computed and experimental vertical settlement time histories (remediation by densification).

(Fig. 22, L1). However, the experiment showed a net settlement of 5 cm at the same location (again reflecting possibly the effect of soil densification).

4.4.3. *Remediation by sheet-pile enclosure*

In this case (Fig. 24), the computed vertical settlements at all selected locations were much less than the experimental results. The lack of adequate densification-induced volumetric strains in the computed results is most evident at location L3 (Fig. 24).

4.5. *Discussion of overall response*

The computational and experimental results presented above systematically reveal a number of liquefaction-related soil response characteristics. Based on these results, two main implications are:

 (i) Post-liquefaction dilation behaviour may play a major role in dictating the soil dynamic response (shear stress-strain in general, and extent of permanent deformation in particular), and
(ii) Observed acceleration response patterns may be good indicators of the different underlying liquefaction response mechanisms.
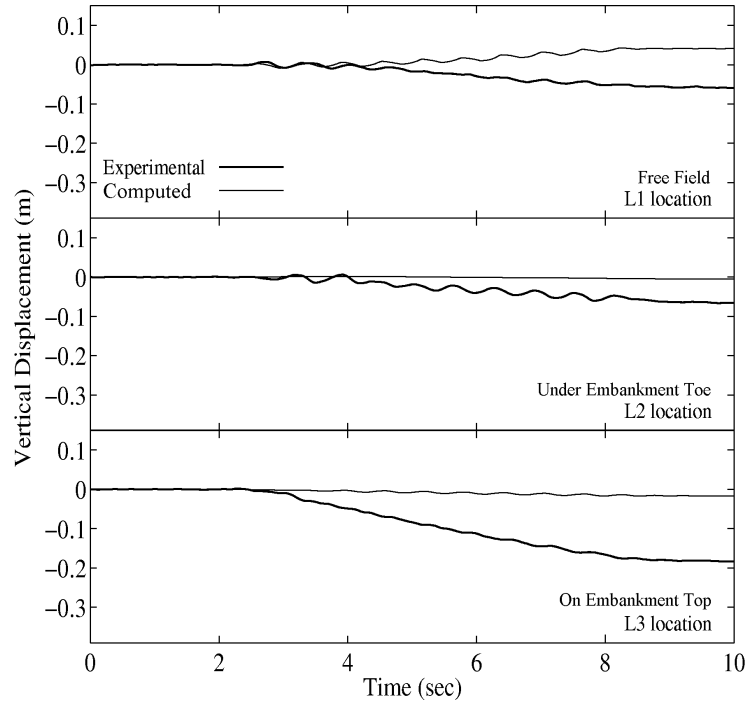
Fig. 24.   Computed and experimental vertical settlement time histories (remediation by sheet-pile enclosure).

For instance, the observed strong asymmetric acceleration spikes (in the first two models) may be associated with significant post-liquefaction dilative response in the "down-slope" direction. Further, the observed steady decay in acceleration amplitudes (in the last model) indicates gradual loss of soil stiffness and strength, with relatively small shear deformation.

In general, the numerical model was able to capture some essential soil response characteristics during liquefaction. In all cases, the computed accelerations were in reasonable agreement with the recorded counterparts. However, significant discrepancies also existed between the computed and experimental results. One noticeable discrepancy is in pore-pressures under the embankment center (P9 in Figs. 11, 16, and 21). During the shaking phase, it is seen that the computed buildup in all three models was higher than the recorded counterpart (especially evident in Figs. 16 and 21). One possible explanation [Adalier, 1996] is based on the experimental observation that major cracks had propagated vertically throughout the embankment body. During the liquefaction process, foundation sand had migrated into these cracks. Thus, fluid/sediment flow through the developed cracks might be among the reasons for the lower recorded pore-pressures below the embankment center. Another discrepancy is in the computed and observed vertical displacements in the free field. As mentioned earlier, this difference may be partially attributed to the

phenomenon of soil densification (high plastic volume change) due to the shaking process. These volumetric strains and their relatively rapid rate of accumulation remain a topic of further studies [Arulanandan and Scott, 1993; 1994].

5. Summary and Conclusions

Overall, the presented investigations may be seen as an integrated effort to (i) incorporate a liquefaction constitutive model into a two phase (solid-fluid), fully coupled Finite Element formulation, and (ii) explore the capabilities and limitations of this computational formulation using a valuable series of centrifuge test results. In general, the numerical model was able to reproduce a wide range of shear response mechanisms encountered during liquefaction. In all cases, the computed accelerations were in good agreement with the recorded counterparts. Computed lateral deformations were also realistic in pattern and amplitude. However, significant discrepancies existed between the computed and recorded pore-pressures (below the embankment) and vertical settlements. These discrepancies point to a need for additional research to gain experimental insights, and to more accurately model the observed liquefaction-induced plastic volumetric strains.

Acknowledgements

References

Adalier, K. [1996] "Mitigation of earthquake induced liquefaction hazards," *Ph.D. Thesis*, Department of Civil Engineering, Rensselaer Polytechnic Institute, Troy, NY.

Adalier, K., Elgamal, A.-W. and Martin, G. R. [1998] "Foundation liquefaction countermeasures for earth embankments," *J. Geotech. Geoenviron. Engrg. ASCE* **124**(6), 500–517.

Arulanandan, K. and Scott, R. F. (Eds.) [1993] *Verification of Numerical Procedures for the Analysis of Soil Liquefaction Problems*, Conference Proceedings, Balkema, Rotterdam, Vol. 1.

Arulanandan, K. and Scott, R. F. (Eds.) [1994] *Verification of Numerical Procedures for the Analysis of Soil Liquefaction Problems*, Conference Proceedings, Balkema, Rotterdam, Vol. 2.

Arulmoli, K., Muraleetharan, K. K., Hossain, M. M. and Fruth, L. S. [1992] "VELACS: Verification of liquefaction analyses by centrifuge studies, laboratory testing program, soil data report," *Report, The Earth Technology Corporation*, Project No. 90-0562, Irvine, CA.

Biot, M. A. [1962] "The mechanics of deformation and acoustic propagation in porous media," *J. Applied Physics* **33**(4), 1482–1498.

Borja, R. I., Chao, H. Y., Montans, F. and Lin, C. H. [1999a] "Nonlinear ground response at Lotung LSST site," *J. Geotech. Geoenviron. Engrg. ASCE* **125**(3), 187–197.

Borja, R. I., Chao, H. Y., Montans, F. and Lin, C. H. [1999b] "SSI effects on ground motion at Lotung LSST site," *J. Geotech. Geoenviron. Engrg. ASCE* **125**(9), 760–770.

Byrne, P. M. and McIntyre, J. [1994] "Deformations in Granular Soils due to Cyclic Loading," *Proceedings of Settlement 94*, ASCE Geotechnical Special Publication No. 40, pp. 1864–1896.

Casagrande, A. [1975] "Liquefaction and cyclic deformation of sands — A critical review," *Proc. 5th Pan-American Conference on Soil Mechanics and Foundation Engineering*, Buenos Aires, Argentina; also published as Harvard Soil Mechanics Series No. 88, January 1976, Cambridge, MA.

Chan, A. H. C. [1988] "A unified finite element solution to static and dynamic problems in geomechanics," *Ph.D. dissertation*, University College of Swansea, U.K.

Cubrinovski, M. and Ishihara, K. [1998] "State concept and modified elastoplasticity for sand modeling," *Soils Foundations* **38**(4), 213–225.

Dobry, R., Taboada, V. and Liu, L. [1997] "Centrifuge modeling of liquefaction effects during earthquakes," *Keynote Lecture, Proc. 1st Int. Conf. Earthq. Geotech. Engrg.*, Ishihara, K. (Ed.), Balkema, Rotterdam, 3, pp. 1291–1324.

Dobry, R. and Abdoun, T. [1998] "Post-triggering response of liquefied sand in the free field and near foundations," *Proc. Geotech. Earthq. Engrg. Soil Dyn. III*, Dakoulas, P., Yegian, M. and Holtz., R. D., (Eds.), Geotechnical Special Publication No. 75, ASCE, 2, pp. 270–300.

Elgamal, A., Lai, T., Yang, Z. and He, L. [2001] "Dynamic soil properties, seismic downhole arrays and applications in practice," (CD-ROM), State-of-the-art paper, *Proc. 4th Int. Conf. Recent Adv. Geotechn. Earthq. Engrg. Soil Dyn.* San Diego, CA, March 26-31, S. Prakash, (Ed.).

Finn, W. D. L., Lee, K. W. and Martin, G. R. [1977] "An effective stress model for liquefaction," *J. Geotech. Engrg. Div. ASCE* **103**, 513–533.

Finn, W. D. L., Ledbetter, R. H. and Marcuson, W. F. [1994] "Seismic deformation in embankment and slopes," *2nd Seismic Short Course on Evaluation and Mitigation of Earthquake Induced Liquefaction Hazards*, U. of Southern California, Los Angeles, CA.

Hill, R. [1950] *The Mathematical Theory of Plasticity*, Oxford Univ. Press, London, U.K.

Iai, S. [1991] "A strain space multiple mechanism model for cyclic behavior of sand and its application, *Earthquake Engineering Research Note No. 43*, Port and Harbor Research Institute, Ministry of Transport, Japan.

Iai, S. [1998] "Seismic analysis and performance of retaining structures," *Proc. Geotech. Earthq. Engrg. Soil Dyn. III*, Dakoulas, P., Yegian, M. and Holtz., R. D., (Eds.), Geotechnical Special Publication No. 75, ASCE, 2, pp. 1020–1044.

Ishihara, K. [1985] "Stability of natural deposits during earthquakes," *Theme Lecture, Proc., 11th Int. Conf. Soil Mech. Foundation Engrg.* Balkema, Rotterdam, 2, pp. 321–376.

Iwan, W. D. [1967] "On a class of models for the yielding behavior of continuous and composite systems," *J. Appl. Mech. ASME* **34**, 612–617.

Kawakami, F. and Asada, A. [1966] "Damage to the ground and earth structures by the Niigata earthquake of June 16, 1964," *Soils Foundations* **6**(1), 14–30.

Kimura, T., Takemura, J., Hiro-oka, A., Okamura, M. and Matsuda T. [1997] "Countermeasures against liquefaction of sand deposits with structures," *Proceedings, 1st Int. Conf. Earthquake Geotechnical Engineering*, Ishihara, K. (Ed.), Balkema, Rotterdam, 3, pp. 1203–1224.

Kramer, S. L. [1996] *Geotechnical Earthquake Engineering*, Prentice Hall Publisher, Upper Saddle River, NJ.

Lacy, S. [1986] "Numerical procedures for nonlinear transient analysis of two-phase soil system," *Ph.D. Dissertation*, Princeton University, NJ.

Lambe, T. W. and Whitman, R. V. [1969] *Soil Mechanics*, John Wiley & Sons, New York.

Ledbetter, R. H., Liam Finn W. D., Hynes, M. E., Nickell, J. S., Allen, M. G. and Stevens, M. G. [1994] "Seismic safety improvement of Mormon Island auxiliary dam," *2nd Seismic Short Course on Evaluation and Mitigation of Earthquake Induced Liquefaction Hazards*, U. of Southern California, Los Angeles, CA.

Li, X. S. and Dafalias, Y. F. [2000] "Dilatancy for cohesionless soils," *Geotechnique* **50**(4), 449–460.

Manzari, M. T. and Dafalias, Y. F. [1997] "A critical state two-surface plasticity model for sands," *Geotechnique* **49**(2), 252–272.

Marcuson, W. F., Hadala, P. F. and Ledbetter, R. H. [1996] "Seismic rehabilitation of earth dams," *J. Geotechnical Engineering ASCE* **122**(1), 7–20.

Matsuo, O. [1996] "Damage to river dikes," *Soils Foundations* **36**(1), 235–240.

McCulloch, D. S. and Bonilla, M. G. [1967] "Railroad damage in the Alaska earthquake," *J. Geotech. Engrg. Div. ASCE* **93**(5), pp. 89–100.

Mroz, Z. [1967] "On the description of anisotropic work hardening," *J. Mech. Phys. Solids* **15**, 163–175.

Muraleetharan, K. K., Mish, K. D. and Arulanandan, K. [1994] "A fully coupled nonlinear dynamic analysis procedure and its verification using centrifuge test results," *Int. J. Num. Anal. Meth. Geomech.* **18**, 305–325.

Nemat-Nasser, S. and Shokooh, A. [1979] "A unified approach to densification and liquefaction of cohesionless sand in cyclic shearing," *Can. Geotech. J.* **16**, 659–678.

Parra, E. [1996] "Numerical modeling of liquefaction and lateral ground deformation including cyclic mobility and dilation response in soil system," *Ph.D. Thesis*, Dept. of Civil Engineering, Rensselaer Polytechnic Institute, Troy, NY.

Pecker, A., Prevost, J. H. and Dormieux, L. [2001] "Analysis of pore pressure generation and dissipation in cohesionless materials during seismic loading," *J. Earthq. Engrg.* **5**(4), 441–464.

Prevost, J. H. [1985] "A simple plasticity theory for frictional cohesionless soils," *Soil Dyn. Earthq. Engrg.* **4**(1), 9–17.

Prevost, J. H. [1989] "DYNA1D, A computer program for nonlinear seismic site response analysis: Technical documentation," *Technical Report NCEER-89-0025*, National Center for Earthquake Engineering Research, State University of New York at Buffalo.

Ragheb, A. [1994] "Numerical analysis of seismically induced deformations in saturated granular soil strata," *Ph.D. Thesis*, Dept. of Civil Engineering, RPI, Troy, NY.

Seed, H. B. [1968] "Landslides during earthquakes due to soil liquefaction," *J. Geotech. Engrg. Div. ASCE* **94**(SM5), 1055–1123.

Seed, H. B. [1970] "Soil problems and soil behavior," Chapter 10 of *Earthquake Engineering*, Wiegel R. L. (Ed.), Prentice-Hall Inc., NJ.

Taboada, V. M. [1995] "Centrifuge modeling of earthquake-induced lateral spreading in sand using a laminar box," *Ph.D. Thesis*, Rensselaer Polytechnic Institute, Troy, NY.

Tan, T. S. and Scott, R. F. [1985] "Centrifuge scaling considerations for fluid-particle systems," *Geotechnique* **35**(4), 461–470.

Tani, S. [1991] "Consideration of earthquake damage to earth dam for irrigation in Japan," *Proc. 2nd Intl. Conf. on Recent Advances in Geotechnical Earthquake Engineering and Soil Dynamics*, S. Prakash, (Ed.), University of Missouri-Rolla, pp. 1137–1142.

Tani, S. [1996] "Damage to earth dams," *Soils Foundations* **36**(1), 263–272.

Vaid, Y. P. and Thomas, J. [1995] "Liquefaction and postliquefaction behavior of sand," *J. Geotech. Engrg. ASCE* **121**(2), 163–173.

Vaid, Y. P. and Sivathayalan, S. [1999] "Fundamental factors affecting liquefaction susceptibility of sands," *Physics and Mechanics of Soil Liquefaction*, Lade, P., Yamamuro, J. (Eds.), Balkema, Rotterdam, pp. 105–120.

Wang, Z. L., Dafalias, Y. F. and Shen, C. K. [1990] "Bounding surface hypoplasticity model for sand," *J. Engrg. Mech. ASCE* **116**, 983–1001.

Yang, Z. [2000] "Numerical modeling of earthquake site response including dilation and liquefaction," *Ph.D. Dissertation*, Dept. of Civil Engineering and Engineering Mechanics, Columbia University, New York, NY.

Zienkiewicz, O. C., Chan, A. H. C., Pastor, M., Paul, D. K. and Shiomi, T. [1990] "Static and dynamic behavior of soils: A rational approach to quantitative solutions: I. Fully saturated problems," *Roy. Soc. London* **A429**, 285–309.